JACS
JOURNAL OF THE AMERICAN CHEMICAL SOCIETY
Article
pubs.acs.org/JACS

Proton-Coupled Electron-Transfer Reduction of Dioxygen Catalyzed by a Saddle-Distorted Cobalt Phthalocyanine

Tatsuhiko Honda,[†] Takahiko Kojima,*[,‡] and Shunichi Fukuzumi*[,†,§]

[†]Department of Material and Life Science, Graduate School of Engineering, Osaka University, ALCA, Japan Science and Technology Agency (JST), Suita, Osaka 565-0871, Japan

[‡]Department of Chemistry, University of Tsukuba, Tsukuba, Ibaraki 305-8571, Japan

[§]Department of Bioinspired Science, Ewha Womans University, Seoul 120-750, Korea

Supporting Information

ABSTRACT: Proton-coupled electron-transfer reduction of dioxygen (O_2) to afford hydrogen peroxide (H_2O_2) was investigated by using ferrocene derivatives as reductants and saddle-distorted (α-octaphenylphthalocyaninato)cobalt(II) ($Co^{II}(Ph_8Pc)$) as a catalyst under acidic conditions. The selective two-electron reduction of O_2 by dimethylferrocene (Me_2Fc) and decamethylferrocene ($Me_{10}Fc$) occurs to yield H_2O_2 and the corresponding ferrocenium ions (Me_2Fc^+ and $Me_{10}Fc^+$, respectively). Mechanisms of the catalytic reduction of O_2 are discussed on the basis of detailed kinetics studies on the overall catalytic reactions as well as on each redox reaction in the catalytic cycle. The active species to react with O_2 in the catalytic reaction is switched from $Co^{II}(Ph_8Pc)$ to protonated $Co^{I}(Ph_8PcH)$, depending on the reducing ability of ferrocene derivatives employed. The protonation of $Co^{II}(Ph_8Pc)$ inhibits the direct reduction of O_2; however, the proton-coupled electron transfer from $Me_{10}Fc$ to $Co^{II}(Ph_8Pc)$ and the protonated $[Co^{II}(Ph_8PcH)]^+$ occurs to produce $Co^{I}(Ph_8PcH)$ and $[Co^{I}(Ph_8PcH_2)]^+$, respectively, which react immediately with O_2. The rate-determining step is a proton-coupled electron-transfer reduction of O_2 by $Co^{II}(Ph_8Pc)$ in the $Co^{II}(Ph_8Pc)$-catalyzed cycle with Me_2Fc, whereas it is changed to the electron-transfer reduction of $[Co^{II}(Ph_8PcH)]^+$ by $Me_{10}Fc$ in the $Co^{I}(Ph_8PcH)$-catalyzed cycle with $Me_{10}Fc$. A single crystal of monoprotonated $[Co^{III}(Ph_8Pc)]^+$, $[Co^{III}Cl_2(Ph_8PcH)]$, produced by the proton-coupled electron-transfer reduction of O_2 by $Co^{II}(Ph_8Pc)$ with HCl, was obtained, and the crystal structure was determined in comparison with that of $Co^{II}(Ph_8Pc)$.

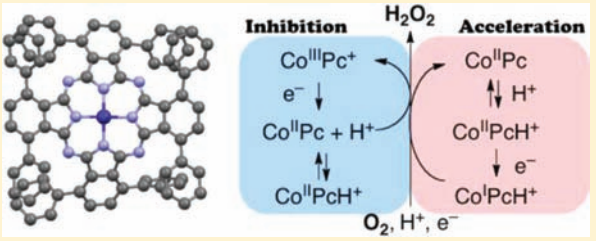

INTRODUCTION

Electron-transfer reactions can be efficiently controlled by proton uptake and release to manipulate redox potentials of an electron donor and/or an electron acceptor. A typical example is a proton-coupled electron transfer, which plays pivotal roles in biological electron-transfer systems such as photosynthesis and respiration.[1−7] Cytochrome *c* oxidases (C*c*O) are the terminal enzymes of respiratory chains, catalyzing the reduction of molecular oxygen to water and at the same time generating a proton gradient across the membrane for proton pumping.[1−3,6,7] In the active site of this enzyme, the reduction of dioxygen is catalyzed by a bimetallic active site consisting of heme and nonheme Cu moieties assisted by the hydroxy group of the neighboring tyrosine connected to a Cu-coordinated imidazole. A number of synthetic models of C*c*O active sites have been reported by using metal complexes of porphyrins and porphyrin analogues for the dioxygen reduction in electrocatalytic and homogeneous systems, because the reduction of dioxygen is not only of biological interest but also of technological importance as fundamentals of fuel cells.[8−27] To gain mechanistic insights into the proton-coupled multielectron redox process in C*c*O active sites, molecular systems such as Pacman and Hangman porphyrins have been extensively studied to control the effective O−O bond cleavage by modifying the peripheral substituents around the dioxygen molecule bound to metal centers.[10−14]

Porphyrin analogues such as phthalocyanines (Pc) have also been applied as ligands of metal complexes acting as catalysts for dioxygen reduction, in particular as electrochemical catalysts.[23−27] The presence of basic nitrogen atoms at meso positions of phthalocyanine provides the possibility of facile modification of its chemical and electronic properties by the protonation of the meso nitrogen atoms. Recently, we have reported the high basicity of saddle-distorted α-octaphenylphthalocyanine (Ph_8Pc) and the enhanced electron-accepting ability of the resulting protonated phthalocyanine (Ph_8PcH^+).[28] Protonated planar (phthalocyaninato)iron(III) has recently been reported as an effective cathode material for a hydrogen peroxide fuel cell operating under acidic conditions.[29] Hydrogen peroxide has merited increasing attention as a promising candidate as a sustainable energy carrier,[30−32] because the free enthalpy change of the decomposition of hydrogen peroxide to water and dioxygen is as large as −210.71 kJ mol^{-1}.[33] Hydrogen peroxide has also been used as a highly efficient and competitive chemical in terms of delignification efficiency and

Received: October 24, 2011
Published: February 2, 2012

dx.doi.org/10.1021/ja209978q | *J. Am. Chem. Soc.* 2012, 134, 4196−4206

reduction of ecological impact.[34,35] However, the catalytic mechanism of protonated metallophthalocyanines has yet to be clarified in the reduction of dioxygen in homogeneous solution. The mechanistic study of the two-electron reduction of dioxygen is essential to develop sustainable systems employing hydrogen peroxide as an energy carrier.

We report herein the catalytic two-electron reduction of dioxygen by using ferrocene derivatives as one-electron reductants with (α-octaphenylphthalocyaninato)cobalt (Co(Ph_8Pc)) as a catalyst under acidic conditions. It has been found that the protonation of $Co^{II}(Ph_8Pc)$ (Scheme 1) in the catalytic

Scheme 1

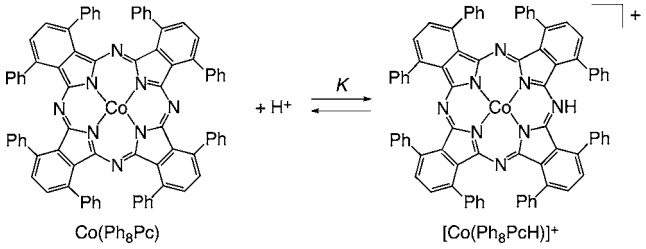

reduction of dioxygen plays dual roles, as discussed in this paper: one is an inhibiting effect on the reaction of $Co^{II}(Ph_8Pc)$ with dioxygen in the case of the Co(II/III) cycle; the other is an acceleration effect on the proton-coupled electron-transfer reduction of $Co^{II}(Ph_8Pc)$ and $[Co^{II}(Ph_8PcH)]^+$ by decamethylferrocene ($Me_{10}Fc$) to produce $Co^{I}(Ph_8PcH)$ and $[Co^{I}(Ph_8PcH_2)]^+$, which readily react with dioxygen in the case of the Co(II/I) cycle. In such a case, the reaction mechanism of the catalytic reduction of dioxygen is switched from the $Co^{II}(Ph_8Pc)$-catalyzed cycle (Co(II/III) cycle) to the protonated $Co^{I}(Ph_8PcH)$-catalyzed cycle (Co(II/I) cycle) depending on the reducing ability of ferrocene derivatives. In addition, the crystal structure of monoprotonated $[Co^{III}(Ph_8Pc)]^+$, $[Co^{III}Cl_2(Ph_8PcH)]$, produced by the proton-coupled electron-transfer reduction of O_2 by $Co^{II}(Ph_8Pc)$ in the presence of HCl, was successfully determined in comparison with that of $Co^{II}(Ph_8Pc)$.

EXPERIMENTAL SECTION

General Procedure. Chemicals were purchased from commercial sources and used without further purification, unless otherwise noted. Benzonitrile (PhCN) used for spectroscopic and electrochemical measurements was distilled over phosphorus pentoxide prior to use.[36] 1,4,8,11,15,18,22,25-Octaphenylphthalocyanine (H_2Ph_8Pc) was synthesized according to the reported procedure.[37] Tetra-*n*-butylammonium hexafluorophosphate ($TBAPF_6$) was twice recrystallized from ethanol and dried in vacuo prior to use. $[Ru(bpy)_3](ClO_4)_3$ (bpy = 2,2′-bipyridine) was prepared from tris(2,2′-bipyridyl)ruthenium(II) chloride hexahydrate by oxidation with PbO_2.[38] ^{1}H NMR spectra (300 MHz) were recorded on a JEOL AL-300 spectrometer at room temperature, and chemical shifts (ppm) were determined relative to the residual solvent peaks. MALDI-TOF-MS measurements were performed on a Kratos Compact MALDI I (Shimadzu) using dithranol as a matrix. UV−vis spectroscopy was carried out on a Hewlett-Packard 8453 diode array spectrophotometer at room temperature using 1 cm cells. EPR measurements were performed on a JEOL JES-RE1XE spectrometer.

Preparation of (1,4,8,11,15,18,22,25-Octaphenylphthalocyaninato)cobalt(II) ($Co^{II}(Ph_8Pc)$). A mixture of H_2Ph_8Pc (500 mg, 0.45 mmol) and $Co(CH_3CO_2)_2{\cdot}4H_2O$ (500 mg, 2.0 mmol) in 300 mL of $CHCl_3/CH_3OH$ (2/1 v/v) was refluxed under nitrogen for 1 h. The residue was dissolved into CH_2Cl_2, and then the solution was washed several times with water and dried over Na_2SO_4. The product was purified by column chromatography on silica gel using CH_2Cl_2 as an eluent and recrystallized from CH_2Cl_2/hexane (361 mg, 66%). UV−vis (PhCN) λ_{max} (ε_{max}): 683 nm (2.9×10^4 M^{-1} cm^{-1}), 760 nm (9.1×10^4 M^{-1} cm^{-1}). MALDI-TOF-MS: m/z 1179.3 (M^+). Anal. Calcd for $C_{80}H_{48}CoN_8$ (Co(Ph_8Pc)): C, 81.41; H, 4.10; N, 9.49. Found: C, 81.15; H, 4.37; N, 9.44. ^{1}H NMR ($CDCl_3$. 300 MHz): δ 10.5 (16H), 9.7 (8H), 8.8 (24H).

Preparation of $[Co^{III}Cl_2(Ph_8PcH)]$. $[Co^{III}Cl_2(Ph_8PcH)]$ was obtained by two-layered recrystallization with addition of CH_3OH on the top of the toluene solution (2.0 mL) of $Co^{II}(Ph_8Pc)$ (20 mg, 0.042 mmol) in the presence of excess hydrochloric acid. The obtained crystals were dried in vacuo. Anal. calcd for $C_{80}H_{49}N_8CoCl_2{\cdot}1.5H_2O$ ($[CoCl_2(Ph_8PcH)]{\cdot}1.5H_2O$): C, 75.12; H, 4.10; N, 8.76. Found: C, 75.31; H, 3.96; N, 8.84.

X-ray Crystallography. Single crystals of $Co^{II}(Ph_8Pc)$ and $[Co^{III}Cl_2(Ph_8PcH)]$ were mounted on a glass capillary with silicon grease. All measurements were performed on a Rigaku Mercury CCD area detector at −150 °C with graphite-monochromated Mo Kα radiation (λ = 0.710 70 Å) up to $2\theta_{max}$ = 54.7°. All calculations were performed using the Crystal Structure crystallographic software package, and structure refinements were made by a direct method using SIR97 for $Co^{II}(Ph_8Pc)$ and SIR2004 for $[Co^{III}Cl_2(Ph_8PcH)]$, respectively.[39,40] The absolute structure of $[Co^{III}Cl_2(Ph_8PcH)]$ was deduced on the basis of the Flack parameter, 0.010(8), using 9240 Friedel pairs.[41] Crystallographic data are summarized in Table 1.

Table 1. X-ray Crystallographic Data for $Co^{II}(Ph_8Pc)$ and $[Co^{III}Cl_2(Ph_8PcH)]$

	$Co^{II}(Ph_8Pc){\cdot}2CH_2Cl_2$	$[Co^{III}Cl_2(Ph_8PcH)]{\cdot}5C_7H_8$
formula	$C_{82}H_{52}Cl_4CoN_8$	$C_{115}H_{89}Cl_{12}CoN_8$
formula wt	1350.11	1712.86
cryst syst	triclinic	orthorhombic
space group	$P\bar{1}$ (No. 2)	$P2_12_12_1$ (No. 19)
T, K	123	123
a, Å	12.050(2)	14.798(1)
b, Å	15.207(3)	21.317(2)
c, Å	17.854(4)	27.914(3)
α, deg	102.894(3)	
β, deg	96.042(3)	
γ, deg	100.331(3)	
V, Å^3	3101.3(11)	8805.7(12)
Z	2	4
no. of rflns measd	21 973	87 608
no. of observns	11 960	20 181
no. of params refined	850	1136
R1[a]	0.0735 ($I > 2\sigma(I)$)	0.0446
wR2[b,c]	0.2006 (all data)	0.0949
GOF	1.068	1.108

[a] $R1 = \sum||F_o| - |F_c||/\sum|F_o|$. [b] $wR2 = [\sum(w(F_o^2 - F_c^2)^2)/\sum w(F_o^2)^2]^{1/2}$. [c] $w = 1/[\sigma^2(F_o^2) + (0.0500P)^2 + 30.0000P$, where $P = (\max(F_o^2, 0) + 2F_c^2)/3$.

Spectroscopic Measurements. The formation constants (log K) of $[Co(Ph_8PcH^+)]$ were determined by using the Hill equation, which analyzes changes of absorption spectra during the titration as a function of the concentration of added acids.[42] The amount of hydrogen peroxide (H_2O_2) formed was determined by titration with iodide ion: a dilute CH_3CN solution (2.0 mL) of the product mixture (20 μL) was treated with an excess amount of NaI and the amount of I_3^- formed was determined by the absorption spectrum (λ_{max} 361 nm, ε = 2.5×10^4 M^{-1} cm^{-1}).[43]

Kinetic Measurements. Kinetic measurements for fast reactions with short half-lifetimes (within 10 s) were performed on a UNISOKU RSP-601 stopped-flow spectrophotometer with an MOS-type high selective photodiode array at 298 K using a Unisoku thermostated cell

dx.doi.org/10.1021/ja209978q | J. Am. Chem. Soc. 2012, 134, 4196−4206

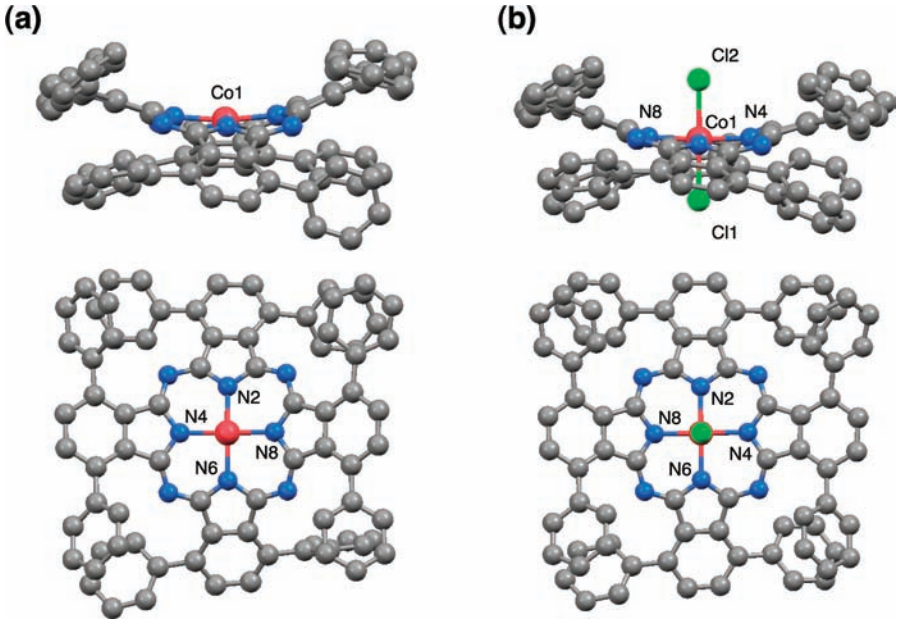

Figure 1. Views of the molecular structures of (a) $Co^{II}(Ph_8Pc)$ and (b) $[Co^{III}Cl_2(Ph_8PcH)]$ from different directions: (gray) carbon; (blue) nitrogen; (red) cobalt; (green) chlorine. Hydrogen atoms and solvent molecules of crystallization are omitted for clarity. Selected bond lengths (Å) of $Co^{II}(Ph_8Pc)$: Co1−N2, 1.881(3); Co1−N4, 1.879(2); Co1−N6, 1.890(3); Co1−N8, 1.891(3). Selected bond lengths (Å) and angles (deg) of $[Co^{III}Cl_2(Ph_8PcH)]$: Co1−N2, 1.909(2); Co1−N4, 1.914(2); Co1−N6, 1.918(2); Co1−N8, 1.910(2); Co1−Cl1, 2.2622(6); Co1−Cl2, 2.2666(6); N2−Co1−Cl1, 87.00(5); N4−Co1−Cl1, 91.29(5); N6−Co1−Cl1, 88.40(5); N8−Co1−Cl1, 93.73(5); N2−Co1−Cl2, 92.15(5); N4−Co1−Cl2, 88.56(5); N6−Co1−Cl2, 92.45(5); N8−Co1−Cl2, 86.42(5).

holder. When stopped-flow measurements were carried out under deaerated or O_2-saturated conditions, a deaerated or O_2-saturated PhCN solution with a stream of argon or O_2 was transferred by means of a glass syringe to a spectrometer cell that was already purged with a stream of argon or O_2. Rate constants of oxidation of ferrocene derivatives by O_2 in the presence of a catalytic amount of $Co^{II}(Ph_8Pc)$ and an excess amount of formic acid in PhCN at 298 K were determined by monitoring the appearance of the absorption band due to the corresponding ferrocenium ions (Fc^+, λ_{max} 620 nm, ε_{max} = 330 M^{-1} cm^{-1}; Me_2Fc^+, λ_{max} 650 nm, ε_{max} = 290 M^{-1} cm^{-1}; Me_8Fc^+, λ_{max} 750 nm, ε_{max} = 410 M^{-1} cm^{-1}; $Me_{10}Fc^+$, λ_{max} 700 nm, ε_{max} = 240 M^{-1} cm^{-1}).[13] At the wavelengths monitored, spectral overlap was observed with $Co^{II}(Ph_8Pc)$ (λ 620 nm (6.7×10^3 M^{-1} cm^{-1}), 650 nm (1.4×10^4 M^{-1} cm^{-1}), 700 nm (2.9×10^4 M^{-1} cm^{-1}), 750 nm (8.3×10^5 M^{-1} cm^{-1})).

Electrochemical Measurements. Cyclic voltammetry (CV) measurements were performed on an ALS 630B electrochemical analyzer, and voltammograms were measured in deaerated PhCN containing 0.10 M $TBAPF_6$ as a supporting electrolyte at room temperature. A conventional three-electrode cell was used with a platinum working electrode (surface area of 0.3 mm^2) and a platinum wire as the counter electrode. The Pt working electrode (BAS) was routinely polished with BAS polishing alumina suspension and rinsed with acetone before use. The potentials were measured with respect to the $Ag/AgNO_3$ (1.0×10^{-2} M) reference electrode. All potentials (vs Ag/Ag^+) were converted to values vs SCE by adding 0.29 V.[44] All electrochemical measurements were carried out under an atmospheric pressure of nitrogen.

RESULTS AND DISCUSSION

Synthesis and Characterization of $Co^{II}(Ph_8Pc)$ and $[Co^{III}Cl_2(Ph_8PcH)]$. $Co^{II}(Ph_8Pc)$ was obtained by a reaction of H_2Ph_8Pc with $Co(CH_3CO_2)_2$. The two-layered recrystallization with addition of *n*-hexane on top of a CH_2Cl_2 solution of $Co^{II}(Ph_8Pc)$ gave a single crystal sufficient for X-ray diffraction. The crystal structure of $Co^{II}(Ph_8Pc)$ was determined to reveal a four-coordinate planar structure, as shown in Figure 1a. Selected bond lengths (Å) are given in the figure caption. A single crystal of monoprotonated $[Co^{III}(Ph_8Pc)]^+$, $[Co^{III}Cl_2(Ph_8PcH)]$, was also obtained by two-layered recrystallization with addition of CH_3OH on top of a toluene solution of $Co^{II}(Ph_8Pc)$ in the presence of an excess amount of HCl. This indicates that $Co^{II}(Ph_8Pc)$ is oxidized by dioxygen in the presence of HCl to produce $[Co^{III}Cl_2(Ph_8PcH)]$. The crystal structure of $[Co^{III}Cl_2(Ph_8PcH)]$ was also determined as depicted in Figure 1b. Selected bond lengths (Å) and angles (deg) are given in the figure caption. In the crystal structure of octahedral $[Co^{III}Cl_2(Ph_8PcH)]$, two chloride ions axially coordinate to the central cobalt ion at distances of 2.2622(6) and 2.2666(6) Å. As shown in Figure 1, both of the crystal structures of $Co^{II}(Ph_8Pc)$ and $[Co^{III}Cl_2(Ph_8PcH)]$ show an out-of-plane distortion because of the steric hindrance among peripheral phenyl groups as well as $Zn(Ph_8Pc)$.[45] To verify the extent of deformation of the phthalocyanine ring, the displacement of each atom from the least-squares mean plane of 24 atoms of the phthalocyanine core (Δrms) in $Co^{II}(Ph_8Pc)$ was calculated to be 0.60 Å, which is nearly the same as that of $Zn(Ph_8Pc)$ (0.59 Å).[28,45] A small relaxation of the ring distortion in $[Co^{III}Cl_2(Ph_8PcH)]$ (Δrms = 0.48 Å) is observed, probably due to elongation of the Co−N bonds as compared to those of $Co^{II}(Ph_8Pc)$.

Protonation Equilibrium of $Co^{II}(Ph_8Pc)$. To examine the protonation of $Co^{II}(Ph_8Pc)$ (Scheme 1), we measured absorption spectral changes upon addition of trifluoromethanesulfonic acid (CF_3SO_3H), trifluoroacetic acid (TFA), and formic acid (HCOOH) in deaerated PhCN. The one-step spectral change was induced by adding 1 equiv of CF_3SO_3H, clearly showing that monoprotonation occurred to form $[Co^{II}(Ph_8PcH)]^+$ (red line in Figure 2b, see also Figure S1 in the Supporting Information). This was also evidenced by the observation of EPR spectral changes upon addition of 1 equiv

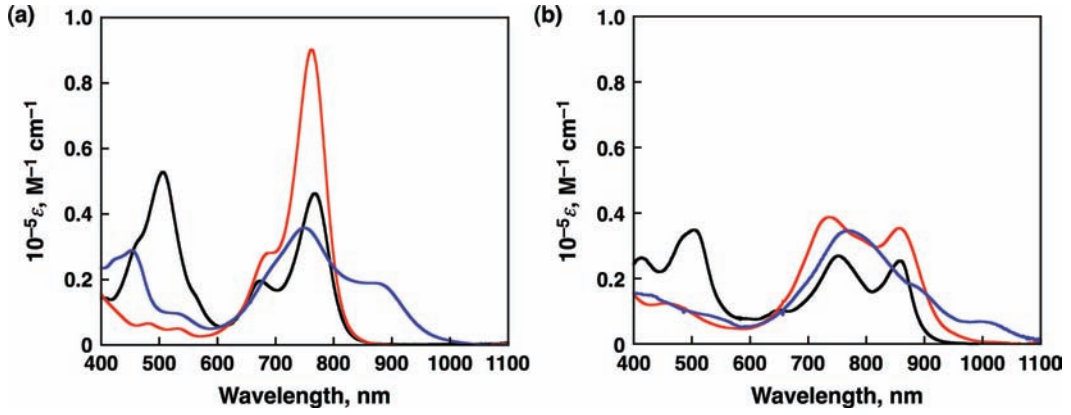

Figure 2. Absorption spectra of (a) $[Co^{I}(Ph_8Pc)]^-$ (black), $Co^{II}(Ph_8Pc)$ (red), and $[Co^{III}(Ph_8Pc)]^+$ (blue) and (b) $Co^{I}(Ph_8PcH)$ (black), $[Co^{II}(Ph_8PcH)]^+$ (red), and $[Co^{III}(Ph_8PcH)]^{2+}$ (blue) in PhCN at 298 K.

of CF_3SO_3H in frozen PhCN at 77 K; $Co^{II}(Ph_8Pc)$ exhibited well-resolved signals at $g_\perp = 2.2896$ and $g_\parallel = 1.9603$ ($A_\perp = 58$ and $A_\parallel = 125$ G, respectively), which are typical for a low-spin ($S = {}^1/_2$) cobalt(II) complex, whereas $[Co^{II}(Ph_8PcH)]^+$ exhibited broader signals at $g_\parallel = 1.9996$ ($A_\parallel = 120$ G) (Figure S2a,b in the Supporting Information). The addition of TFA and HCOOH to a PhCN solution of $Co^{II}(Ph_8Pc)$ afforded the same spectra; however, greater concentrations were required for HCOOH to complete the protonation as compared with those of CF_3SO_3H and TFA. The protonation constants of $[Co^{II}(Ph_8PcH)]^+$ with TFA and HCOOH (log K) were determined by absorption spectral changes to be 2.7 and 0.56, respectively (Figure S1 in the Supporting Information). The lowered basicity of $Co^{II}(Ph_8Pc)$ as compared with that of $Zn^{II}(Ph_8Pc)$ (log $K = 5.1$, TFA, PhCN)[28] can be explained by a decrease in the electron density of the phthalocyanine ring, which is caused by the electronic interaction between the unoccupied $d_{x^2-y^2}$ orbital of the low-spin Co(II) ion and the lone pairs of the phthalocyanine ligand.

Electrochemical measurements on $Co^{II}(Ph_8Pc)$ were performed in deaerated PhCN containing 0.10 M $TBAPF_6$, as shown in Figure 3a. $Co^{II}(Ph_8Pc)$ undergoes three reversible

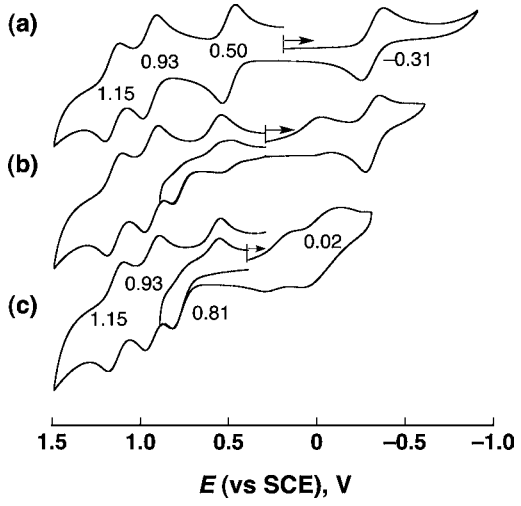

Figure 3. Cyclic voltammograms of (a) $Co^{II}(Ph_8Pc)$, (b) $Co^{II}(Ph_8Pc)$ with 1 equiv of CF_3SO_3H, and (c) $Co^{II}(Ph_8Pc)$ with 2 equiv of CF_3SO_3H in PhCN containing 0.10 M $TBAPF_6$. The concentration of $Co^{II}(Ph_8Pc)$ is 1.0×10^{-3} M.

oxidations and one reversible reduction in PhCN. On the basis of redox potentials of previously characterized Co(II) phthalocyanines,[46,47] the first oxidation and reduction processes are assigned as Co(II)/Co(III) and Co(II)/Co(I) couples, respectively. Thus, the second and third oxidation processes are ascribed to one- and two-electron ligand oxidations. Upon addition of 2 equiv of CF_3SO_3H, the redox potential of Co(II)/Co(I) was positively shifted from −0.31 to 0.02 V (vs SCE). This result clearly shows that the ligand protonation causes the positive shift of the metal-centered redox potential, because the electron-donating ability of the phthalocyanine ligand decreases upon protonation.[28,48] On the other hand, the Co(II)/Co(III) potential was also positively shifted (+0.31 V) by protonation (Figure 3c). The oxidation process of $[Co^{II}(Ph_8PcH)]^+$ becomes irreversible due to the deprotonation of $[Co^{III}(Ph_8PcH)]^+$, because the basicity of the Pc ligand bound to Co(III) is lower than that of the ligand bound to Co(II) due to an increase in the net charge of the metal center.[49] This is consistent with the observation that the ligand oxidation remains unchanged upon addition of 2 equiv of CF_3SO_3H.

The deprotonation of $[Co^{III}(Ph_8PcH)]^+$ is also clarified by the chemical oxidation of $Co^{II}(Ph_8Pc)$ and $[Co^{II}(Ph_8PcH)]^+$ by using $[Ru^{III}(bpy)_3](ClO_4)_3$ as a one-electron oxidant. The one-electron-oxidized species of $Co^{II}(Ph_8Pc)$ and $[Co^{II}(Ph_8PcH)]^+$ exhibited the same spectra, as shown by the blue line in Figure 2a, indicating that the one-electron oxidation of $[Co^{II}(Ph_8PcH)]^+$ produces $[Co^{III}(Ph_8Pc)]^+$ accompanied by deprotonation (see also Figure S3 in the Supporting Information). The oxidation of the Co(II) center in $Co^{II}(Ph_8Pc)$ by the addition of 1 equiv of $[Ru^{III}(bpy)_3](ClO_4)_3$ was evidenced by disappearance of the EPR signal derived from the low-spin Co(II) center of $Co^{II}(Ph_8Pc)$ in PhCN at 77 K and also by the observation of a diamagnetic ^{1}H NMR spectrum in $CDCl_3$ (Figures S3c and 4 in the Supporting Information). We also examined the one-electron reduction of $Co^{II}(Ph_8Pc)$ by using cobaltocene ($CoCp_2$) as a one-electron reductant (Figure S2 in the Supporting Information). The formation of $[Co^{I}(Ph_8Pc)]^-$ was confirmed by observing a characteristic absorption around 500 nm associated with metal-to-ligand charge transfer, as shown by the black line in Figure 2a.[50−55]

The protonation equilibrium between different oxidation states of $[Co(Ph_8Pc)]$ was examined by using TFA in deaerated PhCN, as shown in Figures 2b and 4 (see also Figure S5 in the Supporting Information). In all cases, the protonated species

dx.doi.org/10.1021/ja209978q | J. Am. Chem. Soc. 2012, 134, 4196−4206

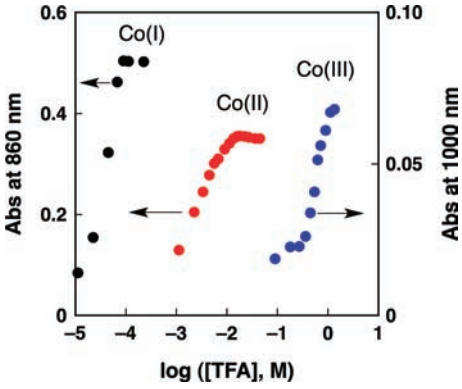

Figure 4. Absorbance changes at 860 (black and red) and 1000 nm (blue) upon addition of TFA to a deaerated PhCN solution of $[Co^{I}(Ph_8Pc)]^-$ (2.0×10^{-5} M, black), $Co^{II}(Ph_8Pc)$ (1.0×10^{-5} M, red), and $[Co^{III}(Ph_8Pc)]^+$ (1.0×10^{-5} M, blue) at 298 K.

showed red-shifted spectra. The formation constants of monoprotonated Co(I), Co(II), and Co(III) Ph_8PcH^+ complexes (log K) were determined by spectroscopic titration to be 4.3, 2.7, and 0.26, respectively, clearly indicating that the basicity of $[Co(Ph_8Pc)]$ decreases on elevating the oxidation states of the cobalt center.[49] This is consistent with the deprotonation of $[Co^{II}(Ph_8PcH)]^+$ upon one-electron oxidation observed in electrochemical measurements.

Catalytic Two-Electron Reduction of O_2 by Ferrocene Derivatives with $Co^{II}(Ph_8Pc)$ in the Presence of an Acid. The addition of $Co^{II}(Ph_8Pc)$ and HCOOH (0.50 M) to an O_2-saturated PhCN solution of Me_2Fc resulted in efficient oxidation of Me_2Fc by O_2. It should be noted that no oxidation of Me_2Fc occurred by O_2 in the absence of $Co^{II}(Ph_8Pc)$. The formation of dimethylferrocenium ion (Me_2Fc^+) was monitored by a rise in absorbance at 650 nm. The black line in Figure 5 shows the time course of formation of Me_2Fc^+ in the

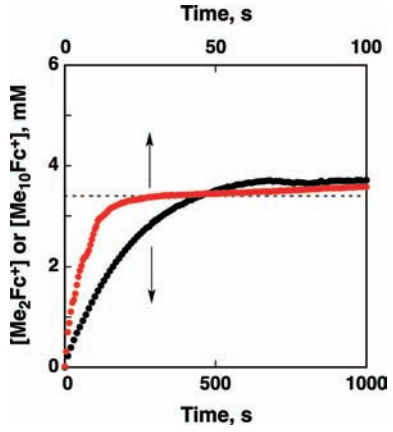

Figure 5. Time profiles of formation of Me_2Fc^+ (black) and $Me_{10}Fc^+$ (red) monitored at 650 nm (ε = 290 M^{-1} cm^{-1}) and 700 nm (ε = 240 M^{-1} cm^{-1}) in electron-transfer oxidation of Me_2Fc or $Me_{10}Fc$ (2.0×10^{-2} M), respectively, with O_2 (1.7×10^{-3} M) catalyzed by $Co^{II}(Ph_8Pc)$ (5.0 and 1.0×10^{-5} M, respectively) in the presence of formic acid (0.50 M) in air-saturated PhCN at 298 K.

reduction of O_2 (1.7×10^{-3} M) in the presence of an excess amount of Me_2Fc (2.0×10^{-2} M), a catalytic amount of $Co^{II}(Ph_8Pc)$ (5.0×10^{-5} M), and a large excess amount of formic acid (0.50 M). The concentration of Me_2Fc^+ (3.4×10^{-3} M) formed in the catalytic reduction of O_2 by Me_2Fc is twice as much as the concentration of O_2 in air-saturated PhCN (1.7×10^{-3} M). This result clearly indicates that the two-electron reduction of O_2 occurs to produce 2 equiv of Me_2Fc^+ (eq 1),

$$2Me_2Fc + O_2 + 2H^+ \xrightarrow[Co^{II}(Ph_8Pc)]{} 2Me_2Fc^+ + H_2O_2 \quad (1)$$

which is consistent with the case for the other mononuclear Co(II) complexes.[13,17] When Me_2Fc was replaced by a stronger one-electron reductant, $Me_{10}Fc$ (E_{ox} = −0.08 V),[13] the clean two-electron reduction of O_2 also occurred to afford $Me_{10}Fc^+$, as shown by the red line in Figure 5. The amount of H_2O_2 formed was determined by the reaction of an excess amount of NaI in CH_3CN (2.0 mL) with the reaction mixture (20 μL: $[Co^{II}(Ph_8Pc)]_0$ = 1.0×10^{-3} M, [HCOOH] = 0.50 M, and $[Me_2Fc]$ or $[Me_{10}Fc]$ = 2.0×10^{-3} M in O_2-saturated PhCN). Under the above conditions, 97 and 74% of H_2O_2 were formed, respectively.

Catalytic Mechanism of the Two-Electron Reduction of O_2 by Me_2Fc with $Co^{II}(Ph_8Pc)$ in the Presence of an Acid. The rate of formation of Me_2Fc^+ in the $Co^{II}(Ph_8Pc)$-catalyzed two-electron reduction of O_2 by Me_2Fc (1.0×10^{-3} M) in the presence of 0.50 M HCOOH in O_2-saturated PhCN obeyed zero-order kinetics, as shown in Figures 6a (see also Figure S6 in the Supporting Information). The zero-order rate constant showed a saturation behavior with increasing concentration of HCOOH (black circles in Figure 6b), which agreed with the absorbance change at 860 nm due to the formation of $[Co^{II}(Ph_8PcH)]^+$ (red circles in Figure 6b). The zero-order rate constant increased linearly with increasing concentrations of $Co^{II}(Ph_8Pc)$ and O_2, as shown in Figure 6c,d, respectively. When Me_2Fc was replaced by a weaker one-electron reductant, Fc (E_{ox} = 0.37 V),[13] the formation of Fc^+ also obeyed zero-order kinetics at the initial stage and the obtained rate constant was virtually the same as that of Me_2Fc (Figure S7a in the Supporting Information). The observed zero-order kinetics indicates that an electron-transfer process involving Me_2Fc is not the rate-determining step in the catalytic cycle of the two-electron reduction of O_2 by Me_2Fc. Instead, proton-coupled electron transfer from $Co^{II}(Ph_8Pc)$, which is in a protonation equilibrium with $[Co^{II}(Ph_8PcH)]^+$, to O_2 to produce $[Co^{III}(Ph_8Pc)]^+$ and $HO_2^\bullet$ may be the rate-determining step in the catalytic cycle, as shown in Scheme 2.

The produced $HO_2^\bullet$ may be rapidly reduced by Me_2Fc with H^+ to afford H_2O_2. On the other hand, $[Co^{III}(Ph_8Pc)]^+$ can also be rapidly reduced by Me_2Fc to regenerate $Co^{II}(Ph_8Pc)$, because Me_2Fc (E_{ox} = 0.26 V vs SCE) lies at a 240 mV overpotential relative to the Co(III/II) couple of $Co(Ph_8Pc)$ (E_{red} = 0.50 V vs SCE), as shown in Scheme 3.

According to Scheme 2, the rate of formation of Me_2Fc^+ is given by eq 2, because electron transfer from Me_2Fc to

$$d[Me_2Fc^+]/dt = 2k_{et}[Co^{II}(Ph_8Pc)][O_2][HCOOH] \quad (2)$$

$[Co^{III}(Ph_8Pc)]^+$ and proton-coupled electron transfer from Me_2Fc to $HO_2^\bullet$ are much faster than proton-coupled electron transfer (k_{et}) from $Co^{II}(Ph_8Pc)$ to O_2, when 2 equiv of Me_2Fc^+ is formed by the rate-determining proton-coupled electron transfer from $Co^{II}(Ph_8Pc)$ to O_2. From the protonation equilibrium in Scheme 1, the concentration of $Co^{II}(Ph_8Pc)$ is given by eq 3, where $[Co^{II}(Ph_8Pc)]_0$ is the initial concentration

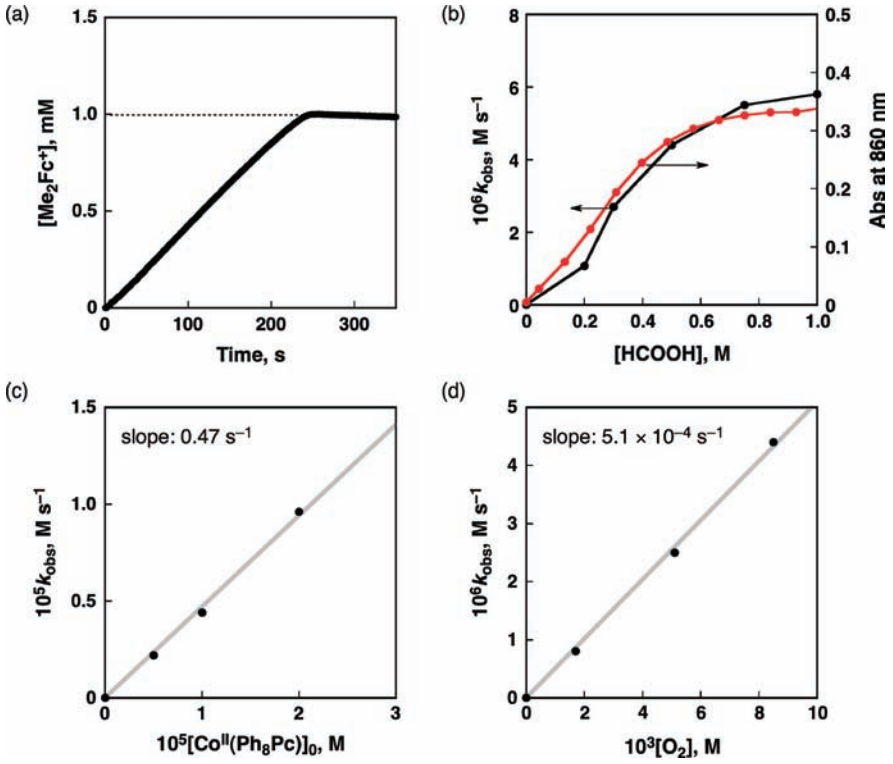

Figure 6. (a) Time profile of the formation of Me_2Fc^+ monitored by absorbance at 650 nm (ε = 290 M^{-1} cm^{-1}) in electron-transfer oxidation of Me_2Fc (1.0×10^{-3} M) by O_2 (8.5×10^{-3} M) catalyzed by $Co^{II}(Ph_8Pc)$ (1.0×10^{-5} M) in the presence of 0.50 M formic acid in PhCN. (b) Plots of k_{obs} (black) and absorbance changes at 860 nm due to $[Co^{II}(Ph_8PcH)]^+$ (red) vs [HCOOH]. (c) Plot of k_{obs} vs $[Co^{II}(Ph_8Pc)]_0$; [HCOOH] = 0.50 M. (d) Plot of k_{obs} vs $[O_2]$.

Scheme 2

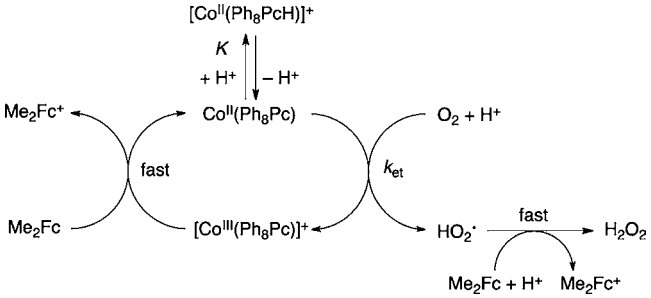

Scheme 3

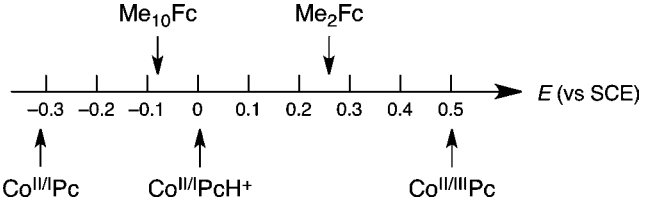

of $Co^{II}(Ph_8Pc)$ and K is the protonation constant with HCOOH (K = 3.6 M^{-1} at 298 K, vide supra). By combining eqs 2 and 3, eq 4 is obtained. It should be noted that

$$[Co^{II}(Ph_8Pc)] = [Co^{II}(Ph_8Pc)]_0/(1 + K[HCOOH]) \quad (3)$$

$$\frac{d[Me_2Fc^+]}{dt} = \frac{2k_{et}[Co^{II}(Ph_8Pc)]_0[O_2][HCOOH]}{1 + K[HCOOH]} \quad (4)$$

$[Co^{II}(Ph_8Pc)]_0/(1 + K[HCOOH])$ in eq 2 corresponds to the concentration of unprotonated $Co^{II}(Ph_8Pc)$, which acts as the actual electron donor. Equation 4 agreed well with the experimental observations in Figure 6, where the rate of formation of Me_2Fc^+ was independent of concentration of Me_2Fc (zero order), and the zero-order rate constant was proportional to the initial concentrations of $Co^{II}(Ph_8Pc)$ and O_2. The saturation behavior of the zero-order rate constant with respect to the concentration of HCOOH (Figure 6b) results from the protonation equilibrium of $Co^{II}(Ph_8Pc)$, when only unprotonated $Co^{II}(Ph_8Pc)$ acts as an electron donor in the proton-coupled electron transfer to O_2, because the Co(II)/Co(III) potential is positively shifted (+0.31 V) by the protonation (Figure 3c). From the results in Figure 6c,d and eq 4, the k_{et} value of proton-coupled electron transfer from $Co^{II}(Ph_8Pc)$ to O_2 in the presence of 0.50 M HCOOH is determined to be $(1.4 \pm 0.1) \times 10^2$ M^{-2} s^{-1} at 298 K.

Proton-Coupled Electron Transfer from $Co^{II}(Ph_8Pc)$ to O_2. The rate-determining step in the catalytic cycle for the two-electron reduction of O_2 by Me_2Fc was examined independently (vide infra). In the presence of an excess amount of HCOOH, proton-coupled electron transfer from $Co^{II}(Ph_8Pc)$ to O_2 occurs to produce $[Co^{III}(Ph_8Pc)]^+$, as shown in Figure 7a, where the final absorption spectrum (red) is the same as that of $[Co^{III}(Ph_8Pc)]^+$ in Figure 2a (blue). The formation of $[Co^{III}(Ph_8Pc)]^+$ was also confirmed by the disappearance of the EPR signal derived from $Co^{II}(Ph_8Pc)$ after the reaction with O_2 (Figure S2d in the Supporting Information). This suggests that the two-electron reduction of O_2 is achieved by 2 equiv of $Co^{II}(Ph_8Pc)$. As shown in Scheme 4, the uphill nature of the proton-coupled electron transfer from $Co^{II}(Ph_8Pc)$ to O_2 (k_{et}) implies that the complex of $[Co^{III}(Ph_8Pc)]^+$ and hydroperoxyl

dx.doi.org/10.1021/ja209978q | J. Am. Chem. Soc. 2012, 134, 4196–4206

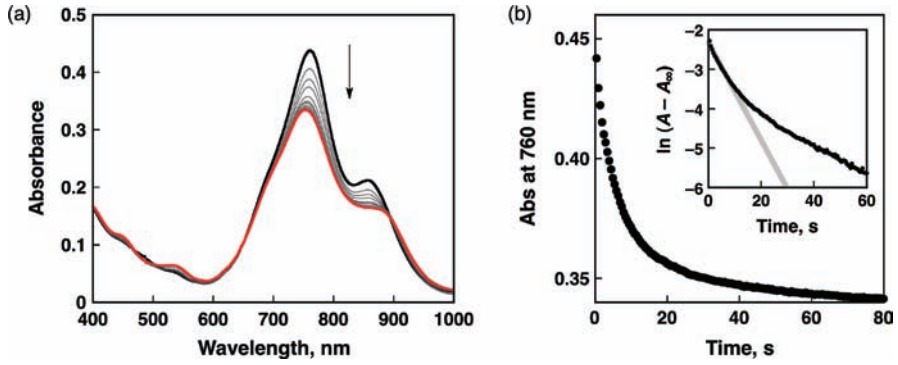

Figure 7. (a) Absorption spectral changes of $Co^{II}(Ph_8Pc)$ (1.0×10^{-5} M) in the presence of formic acid (0.50 M) in O_2-saturated PhCN. (b) Time profiles of absorbance at 760 nm. Inset: first-order plot.

Scheme 4

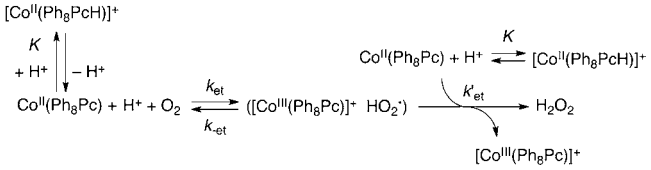

radical ($HO_2^{\bullet}$) ($[Co^{III}(Ph_8Pc)]^+ HO_2^{\bullet}$) undergoes the reverse reaction (k_{-et}) in competition with the subsequent proton-coupled electron transfer from $Co^{II}(Ph_8Pc)$ to yield H_2O_2 and 2 equiv of $[Co^{III}(Ph_8Pc)]^+$.

In such a case, the decay rate of $Co^{II}(Ph_8Pc)$ is given by eq 5, where k_{et} is the rateconstant of proton-coupled electron transfer

$$-d[Co^{II}(Ph_8Pc)]/dt = k_{et}[Co^{II}(Ph_8Pc)][O_2][HCOOH] - k_{-et}[C] + k'_{et}[Co^{II}(Ph_8Pc)][HCOOH][C] \quad (5)$$

from $Co^{II}(Ph_8Pc)$ to O_2, k_{-et} is the rate constant of the reverse reaction, k'_{et} is the rate constant of proton-coupled electron transfer from $Co^{II}(Ph_8Pc)$ to $HO_2^{\bullet}$, K is the protonation constant of $Co^{II}(Ph_8Pc)$ with HCOOH, and [C] corresponds to the concentration of the complex ($[Co^{III}(Ph_8Pc)]^+ HO_2^{\bullet}$) in Scheme 4. The rate of formation of the complex ($[Co^{III}(Ph_8Pc)]^+HO_2^{\bullet}$) is given by eq 6. By subtracting eq 6

$$d[C]/dt = k_{et}[Co^{II}(Ph_8Pc)][O_2][HCOOH] - k_{-et}[C] - k'_{et}[Co^{II}(Ph_8Pc)][HCOOH][C] \quad (6)$$

from eq 5, eq 7 is obtained. Because [C] remains nearly constant during the reaction, [C] is given by eq 8 by applying

$$-d[Co^{II}(Ph_8Pc)]/dt - d[C]/dt = 2k'_{et}[Co^{II}(Ph_8Pc)][HCOOH][C] \quad (7)$$

$$[C] = k_{et}[Co^{II}(Ph_8Pc)][O_2][HCOOH]/(k_{-et} + k'_{et}[Co^{II}(Ph_8Pc)][HCOOH]) \quad (8)$$

the steady-state approximation. The decay rate of $Co^{II}(Ph_8Pc)$ in the proton-coupled electron transfer from $Co^{II}(Ph_8Pc)$ to O_2 is derived from eqs 7 and 8 as shown in eq 9. As expected from eq 9, the decay rate does not obey simple first-order kinetics, as shown in Figure 7b.

$$-\frac{d[Co^{II}(Ph_8Pc)]}{dt} = \frac{2k_{et}k'_{et}[Co^{II}(Ph_8Pc)]^2[O_2][HCOOH]^2}{k_{-et} + k'_{et}[Co^{II}(Ph_8Pc)][HCOOH]} \quad (9)$$

The first-order rate constant (k_{obs}) taken from the initial slope in the first-order plots is given from eqs 3 and 9 by eq 10.

$$k_{obs} = \{2k_{et}k'_{et}[Co^{II}(Ph_8Pc)]_0[O_2][HCOOH]^2/(1 + K[HCOOH])^2\}/\{k_{-et} + k'_{et}[Co^{II}(Ph_8Pc)]_0[HCOOH]/(1 + K[HCOOH])\} \quad (10)$$

The k_{obs} value increased linearly with increasing concentration of O_2 (Figure 8a) as expected by eq 10. The k_{obs} values exhibited saturation behaviors with increasing concentrations of HCOOH and $Co^{II}(Ph_8Pc)$, as shown in Figure 8b,c, respectively, which were consistent with eq 4. In order to determine the k_{et} value, eq 10 is rewritten by eq 11, which

$$k_{obs}^{-1} = \{k_{-et}[Co^{II}(Ph_8Pc)]_0^{-1} + k'_{et}[HCOOH](1 + K[HCOOH])\}/\{2k_{et}k'_{et}[O_2][HCOOH]^2/(1 + K[HCOOH])^2\} \quad (11)$$

predicts a linear correlation between k_{obs}^{-1} and $([Co^{II}(Ph_8Pc)]_0)^{-1}$. The linear correlation between k_{obs}^{-1} and $([Co^{II}(Ph_8Pc)]_0)^{-1}$ was obtained as shown in Figure S8 in the Supporting Information. The inverse of the intercept is given by eq 12, which corresponds to the formation rate of Me_2Fc^+

$$(\text{intercept})^{-1} = \frac{2k_{et}[O_2][HCOOH]}{1 + K[HCOOH]} \quad (12)$$

under the catalytic conditions (eq 4). The k_{et} value was determined from the intercept of the linear plot of k_{obs}^{-1} vs $([Co^{II}(Ph_8Pc)]_0)^{-1}$ to be $(1.6 \pm 0.3) \times 10^2$ M^{-2} s^{-1}, which agreed well with the k_{et} value ($(1.4 \pm 0.1) \times 10^2$ M^{-2} s^{-1})

dx.doi.org/10.1021/ja209978q | J. Am. Chem. Soc. 2012, 134, 4196−4206

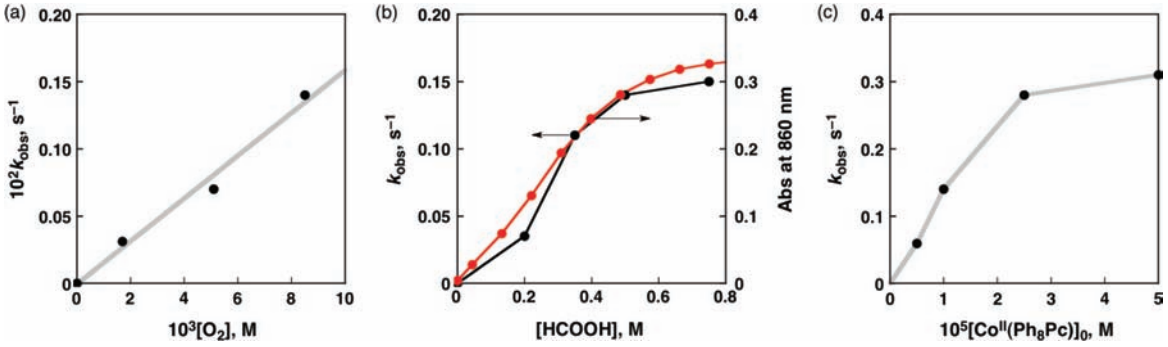

Figure 8. (a) Plot of k_{obs} vs $[O_2]$; $[Co^{II}(Ph_8Pc)] = 1.0 \times 10^{-5}$ M and [HCOOH] = 0.50 M. (b) Plots of k_{obs} (black) and absorbance changes at 860 nm due to $[Co^{II}(Ph_8PcH)]^+$ (red) vs [HCOOH]; $[Co^{II}(Ph_8Pc)] = 1.0 \times 10^{-5}$ M and $[O_2] = 8.5 \times 10^{-3}$ M. (c) Plot of k_{obs} vs $[Co^{II}(Ph_8Pc)]_0$; [HCOOH] = 0.50 M and $[O_2] = 8.5 \times 10^{-3}$ M.

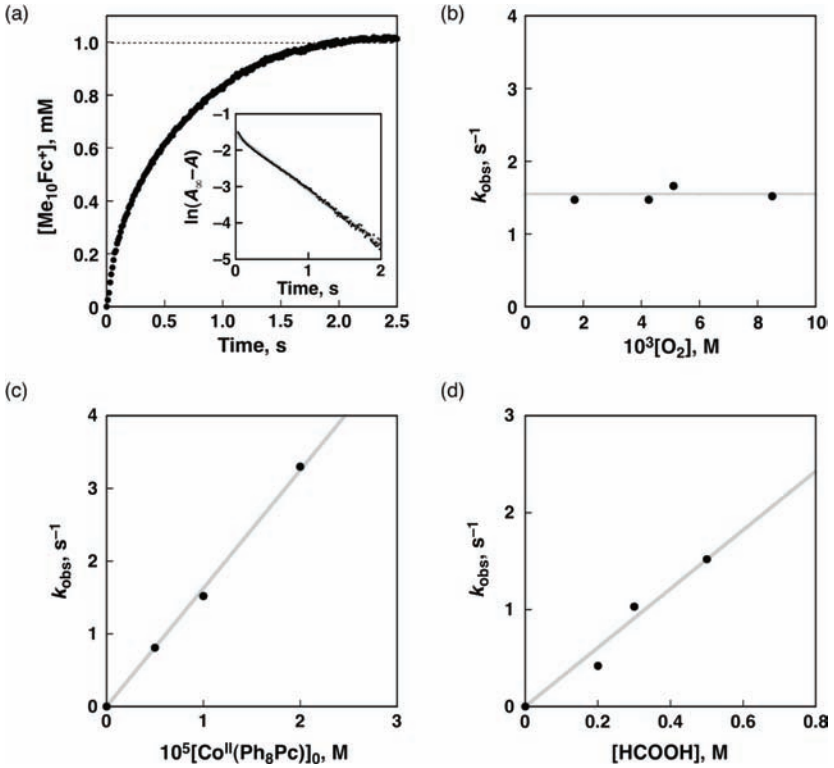

Figure 9. (a) Time profile of formation of $Me_{10}Fc^+$ monitored by absorbance at 700 nm (ε = 240 M^{-1} cm^{-1}) in electron-transfer oxidation of $Me_{10}Fc$ (1.0×10^{-3} M) by O_2 (8.5×10^{-3} M) catalyzed by $Co^{II}(Ph_8Pc)$ (1.0×10^{-5} M) in the presence of formic acid (0.50 M) in PhCN. Inset: first-order plot. (b) Plot of k_{obs} vs $[O_2]$. (c) Plot of k_{obs} vs $[Co^{II}(Ph_8Pc)]_0$. (d) Plot of k_{obs} vs [HCOOH].

determined from the catalytic conditions (Figure 6c,d). Such agreement of the k_{et} values determined from the single-turnover conditions and catalytic conditions supports strongly that the rate-determining step in the catalytic cycle in Scheme 2 is indeed the proton-coupled electron transfer from $Co^{II}(Ph_8Pc)$ to O_2.

In the presence of TFA (pK_a = 0) instead of formic acid (pK_a = 3.77), the two-electron reduction of O_2 occurred in a way similar to that for the case of formic acid. However, no electron transfer occurred in the presence of acetic acid (pK_a = 4.76) (Figure S9 in the Supporting Information).[56] This sharp contrast may stem from the relation among the pK_a values of superoxide anion ($O_2^{\bullet-}$, pK_a = 4.69)[57] and those of acids mentioned above, suggesting that the protonation of $O_2^{\bullet-}$ is indispensable to promote the electron transfer from $Co^{II}(Ph_8Pc)$ to O_2.

Catalytic Mechanism of the Two-Electron Reduction of O_2 by $Me_{10}Fc$ with $Co^{II}(Ph_8Pc)$ in the Presence of an Acid. When $Me_{10}Fc$ was used as a one-electron reductant instead of Me_2Fc, the formation of $Me_{10}Fc^+$ in the catalytic two-electron reduction of O_2 by $Me_{10}Fc$ with $Co^{II}(Ph_8Pc)$ in the presence of HCOOH was completed within a few seconds. Thus, we performed stopped-flow measurements to analyze the kinetics. The rate of formation of $Me_{10}Fc^+$ obeyed pseudo-first-order kinetics (Figure 9a), and the pseudo-first-order rate constant remained constant irrespective of O_2 concentration (Figure 9b). Such independence of the pseudo-first-order rate constant (k_{obs}) of the concentration of O_2 is in sharp contrast to the case of Me_2Fc described above, in which the zero-order rate constant shows a linear dependence on the concentration of O_2 (Figure 7d). This indicates that the proton-coupled electron transfer from $Co^{II}(Ph_8Pc)$ to O_2 is not the rate-determining

dx.doi.org/10.1021/ja209978q | J. Am. Chem. Soc. 2012, 134, 4196–4206

step but that the proton-coupled one-electron reduction of $Co^{II}(Ph_8Pc)$ and $[Co^{II}(Ph_8PcH)]^+$ by $Me_{10}Fc$ may be the rate-determining step, as shown in Scheme 5, because $Me_{10}Fc$

Scheme 5

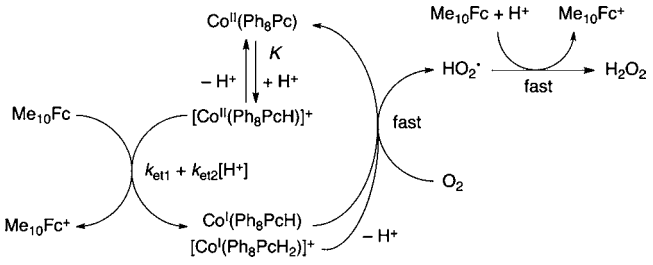

possess only 100 mV overpotential relative to the Co(II/I) couple (Scheme 3). The rate-determining one-electron reduction of $[Co^{II}(Ph_8PcH)]^+$ by $Me_{10}Fc$ may be followed by rapid reduction of O_2 by $Co^{I}(Ph_8PcH)$ and $[Co^{I}(Ph_8PcH_2)]^+$ and the subsequent rapid proton-coupled one-electron reduction of $HO_2^{\bullet}$ by $Me_{10}Fc$ to yield $Me_{10}Fc^+$ and H_2O_2. When $Me_{10}Fc$ was replaced by a weaker one-electron reductant, Me_8Fc, the rate constant of the formation of Me_8Fc^+ also obeyed first-order kinetics, but the k_{obs} value was smaller as compared with the value of $Me_{10}Fc^+$ under the same experimental conditions (Figure S7b in the Supporting Information), as expected from the less negative one-electron oxidation potential of Me_8Fc (E_{ox} = −0.04 V) as compared with $Me_{10}Fc$ (E_{ox} = −0.08 V vs SCE). This also indicates that the rate-determining step is the proton-coupled electron-transfer reduction of $Co^{II}(Ph_8Pc)$ and $[Co^{II}(Ph_8PcH)]^+$ by $Me_{10}Fc$ to produce $Co^{I}(Ph_8PcH)$ and $[Co^{I}(Ph_8PcH_2)]^+$, respectively.

According to Scheme 5, the rate of formation of $Me_{10}Fc^+$ is given by eq 13, because electron transfer from $Co^{I}(Ph_8PcH)$

$$d[Me_{10}Fc^+]/dt = 2(k_{et1} + k_{et2}[HCOOH])[Me_{10}Fc][[Co^{II}(Ph_8PcH)]^+] \quad (13)$$

and $[Co^{I}(Ph_8PcH_2)]^+$ to O_2 and proton-coupled electron transfer from $Me_{10}Fc$ to $HO_2^{\bullet}$ are much faster than electron transfer from $Me_{10}Fc$ to $[Co^{II}(Ph_8PcH)]^+$ to produce $Co^{I}(Ph_8PcH)$ (k_{et1}) and proton-coupled electron transfer from $Me_{10}Fc$ to $[Co^{II}(Ph_8PcH)]^+$ to produce $[Co^{I}(Ph_8PcH_2)]^+$ (k_{et2}[HCOOH]), when 2 equiv of $Me_{10}Fc^+$ is formed. According to the protonation equilibrium in Scheme 1, the concentration of $[Co^{II}(Ph_8PcH)]^+$ in eq 13 is given by eq 14.

$$[[Co^{II}(Ph_8PcH)]^+] = K[Co^{II}(Ph_8Pc)]_0[HCOOH]/(1 + K[HCOOH]) \quad (14)$$

$$d[Me_{10}Fc^+]/dt = \{2(k_{et1} + k_{et2}[HCOOH])K[HCOOH][Me_{10}Fc][Co^{II}(Ph_8Pc)]_0\}/\{1 + K[HCOOH]\} \quad (15)$$

From eqs 13 and 14, eq 15 is obtained. The kinetic formulation derived from Scheme 5 (eq 15) agrees with the experimental observations in Figure 9, where the rate of formation of $Me_{10}Fc^+$ obeyed pseudo-first-order kinetics (first order with respect to concentration of $Me_{10}Fc$; Figure 9a), the k_{obs} value was independent of concentration of O_2 (Figure 9b), but proportional to the initial concentration of $Co^{II}(Ph_8Pc)$ (Figure 9c). The k_{obs} value increased with increasing concentration of HCOOH without exhibiting a saturation behavior, as expected from eq 15. From Figure 9b, c, the second-order rate constant of the proton-coupled electron transfer from $Me_{10}Fc$ to $Co^{II}(Ph_8Pc)$ and $[Co^{II}(Ph_8PcH)]^+$ in the presence of 0.50 M HCOOH was determined to be $(1.6 \pm 0.1) \times 10^5$ M^{-1} s^{-1} at 298 K.

Proton-Coupled Electron Transfer from $Me_{10}Fc$ to $[Co^{II}(Ph_8PcH)]^+$. The rate-determining step in the catalytic cycle for the two-electron reduction of O_2 by $Me_{10}Fc$ with $[Co^{II}(Ph_8PcH)]^+$ in Scheme 5 was studied independently without O_2 (vide infra). Because the electrochemical study revealed that the reduction potential of $Co^{II}(Ph_8Pc)$ was positively shifted by the protonation to 0.02 V vs SCE, electron transfer from $Me_{10}Fc$ (E_{ox} = −0.08 V vs SCE) to $[Co^{II}(Ph_8PcH)]^+$ is energetically feasible (Scheme 3). Indeed, electron transfer from $Me_{10}Fc$ to $[Co^{II}(Ph_8PcH)]^+$ occurs in the presence of HCOOH (0.50 M) in PhCN at 298 K. It should be noted that no electron transfer from $Me_{10}Fc$ to $Co^{II}(Ph_8Pc)$ (E_{red} = −0.31 V, Figure 3a) occurred without HCOOH. The absorption spectral change in the electron-transfer reaction was monitored by using a stopped-flow technique as shown in Figure 10a, where the absorption band at 505 nm due to $Co^{I}(Ph_8PcH)$ appeared, accompanied by a decrease in the absorption band at 760 nm due to $Co^{II}(Ph_8Pc)$ and $[Co^{II}(Ph_8PcH)]^+$. The observed rate constant was determined by the decay of $Co^{II}(Ph_8Pc)$ monitored from a decrease in absorbance at 760 nm, which coincides with formation of $Co^{I}(Ph_8PcH)$, monitored by an increase in absorbance at 505 nm (inset of Figure 10a). The observed rate constant obeyed pseudo-first-order kinetics in the presence of a large excess of $Me_{10}Fc$, and the observed rate constants (k_{obs}) increased with increasing concentration of $Me_{10}Fc$ (Figure 10c). The k_{obs} value also increased with increasing concentration of HCOOH without exhibiting a saturation behavior, as expected from the protonation equilibrium of $Co^{II}(Ph_8Pc)$ (K = 3.6 M^{-1}), as shown in Figure 10b.[58] This is attributed to further protonation to produce diprotonated $[Co^{I}(Ph_8PcH_2)]^+$ in the presence of large concentrations of HCOOH, as shown in Scheme 6 (vide supra, Figure S10 in the Supporting Information).

According to Scheme 6, the decay rate of $[Co^{II}(Ph_8PcH)]^+$ is given by eq 16. Thus, the second-order rate constant of the

$$-d[[Co^{II}(Ph_8PcH)]^+]/dt = (k_{et1} + k_{et2}[HCOOH])[[Co^{II}(Ph_8PcH)]^+][Me_{10}Fc] \quad (16)$$

proton-coupled electron transfer from $Me_{10}Fc$ to $Co^{II}(Ph_8Pc)$ and $[Co^{II}(Ph_8PcH)]^+$ in the presence of 0.50 M HCOOH was determined from the slope of the linear plot of k_{obs} vs $[Me_{10}Fc]$ to be $(1.1 \pm 0.2) \times 10^5$ M^{-1} s^{-1}. By using this value, the observed second-order rate constant under the catalytic conditions with 0.50 M HCOOH in the presence of O_2, which corresponds to $2(k_{et1} + k_{et2}[HCOOH])K[HCOOH]/(1 + K[HCOOH])$ in eq 15, was determined to be $(1.7 \pm 0.3) \times 10^5$ M^{-1} s^{-1}, which agreed well with the experimental value

dx.doi.org/10.1021/ja209978q | J. Am. Chem. Soc. 2012, 134, 4196–4206

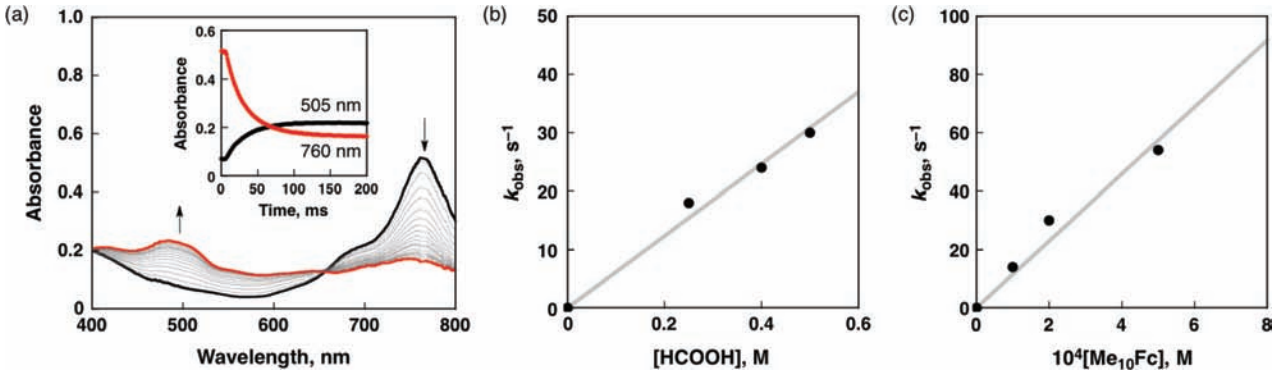

Figure 10. (a) Absorption spectral changes of $Co^{II}(Ph_8Pc)$ (1.0×10^{-5} M) in the presence of formic acid (0.50 M) and $Me_{10}Fc$ (2.0×10^{-4} M) in deaerated PhCN. Inset: time profiles of absorbance at 505 (black) and 760 nm (red) to $Co^{I}(Ph_8PcH)$ and $Co^{II}(Ph_8Pc)$, respectively. (b) Plot of k_{obs} vs [HCOOH]; $[Co^{II}(Ph_8Pc)] = 1.0 \times 10^{-5}$ M and $[Me_{10}Fc] = 2.0 \times 10^{-4}$ M. (c) Plot of k_{obs} vs $[Me_{10}Fc]$; $[Co^{II}(Ph_8Pc)] = 1.0 \times 10^{-5}$ M and [HCOOH] = 0.50 M.

Scheme 6

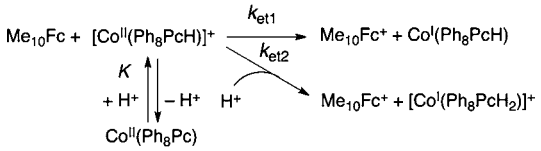

($(1.6 \pm 0.1) \times 10^5$ M^{-1} s^{-1}) obtained from the slopes in Figure 9b,c (vide supra). Such agreement strongly indicates that the rate-determining step in the catalytic cycle in Scheme 5 is indeed the proton-coupled electron transfer from $Me_{10}Fc$ to $Co^{II}(Ph_8Pc)$ and $[Co^{II}(Ph_8PcH)]^+$, respectively (Scheme 6).

SUMMARY AND CONCLUSION

The present study has demonstrated the protonation of $Co^{II}(Ph_8Pc)$ significantly enhances the catalytic two-electron reduction of O_2 by a ferrocene derivative in the presence of an acid. The X-ray crystal structure of the protonated $Co^{II}(Ph_8Pc)$ ($[Co^{II}(Ph_8PcH)]^+$) was successfully determined in comparison with that of $Co^{II}(Ph_8Pc)$. The protonation of $Co^{II}(Ph_8Pc)$ has been found to inhibit the direct reduction of O_2 due to the elevation of the Co(II)/Co(III) redox potential of the Co(II) center, whereas the proton-coupled electron transfer from $Me_{10}Fc$ to $Co^{II}(Ph_8Pc)$ and $[Co^{II}(Ph_8PcH)]^+$ becomes possible by the protonation of $Co^{II}(Ph_8Pc)$ to produce $Co^{I}(Ph_8PcH)$ and $[Co^{I}(Ph_8PcH_2)]^+$, respectively, which readily reduce dioxygen. When $Me_{10}Fc$ was replaced by a weaker species such as Me_2Fc, the proton-coupled electron transfer from Me_2Fc to $[Co^{II}(Ph_8PcH)]^+$ became energetically impossible, but instead proton-coupled electron transfer from $Co^{II}(Ph_8Pc)$ to O_2 occurred to produce $[Co^{III}(Ph_8Pc)]^+$, which is rapidly reduced by Me_2Fc to regenerate $Co^{II}(Ph_8Pc)$. Thus, the catalytic pathway is switched from the Co(II/I) cycle to the Co(II/III) cycle by increasing the reducing ability of the one-electron reductant for the catalytic two-electron reduction of O_2 in the presence of an acid. Such a switch of the catalytic mechanism for the proton-coupled O_2 reduction provides deeper insights toward the development of more efficient catalysts for selective two-electron reduction of O_2 to produce hydrogen peroxide, which is a promising candidate for a renewable energy source.[30−32]

ASSOCIATED CONTENT

Supporting Information

Text, figures, and CIF files giving absorption titration, time course of kinetic measurements, and electrochemical measurement data, ^{1}H NMR and EPR spectra, and crystal structure data. This material is available free of charge via the Internet at http://pubs.acs.org.

AUTHOR INFORMATION

Corresponding Author

*E-mail: kojima@chem.tsukuba.ac.jp (T.K.); fukuzumi@chem.eng.osaka-u.ac.jp (S.F.).

Notes

The authors declare no competing financial interest.

ACKNOWLEDGMENTS

This work was supported by a Grant-in-Aid (No. 20108010) from the Ministry of Education, Culture, Sports, Science and Technology of Japan (to S.F.), NRF/MEST of Korea through WCU (R31-2008-000-10010-0) and GRL (2010-00353) Programs (to S.F.). T.H. appreciates support from the Global COE program "Global Education and Research Center for Bio-Environmental Chemistry" of Osaka University and a JSPS fellowship for young scientists.

REFERENCES

(1) Takahashi, E.; Wraight, C. A. *Biochemistry* **1992**, *31*, 855.
(2) (a) Ferguson-Miller, S.; Babcock, G. T. *Chem. Rev.* **1996**, *96*, 2889. (b) Babcock, G. T.; Wikström, M. *Nature* **1992**, *356*, 301. (c) Babcock, G. T. *Proc. Natl. Acad. Sci. U.S.A.* **1999**, *96*, 12971. (d) Kaila, V. R. I.; Verkhovsky, M. I.; Wikström, M. *Chem. Rev.* **2010**, *110*, 7062.
(3) Stowell, M. H. B.; McPhillips, T. M.; Rees, D. C.; Soltis, S. M.; Abresch, E.; Feher, G. *Science* **1997**, *276*, 812.
(4) Rotello, V. M. In *Electron Transfer in Chemistry*; Balzani, V., Ed.; Wiley-VCH: Weinheim, Germany, 2001.
(5) (a) Costentin, C.; Robert, M.; Savéant, J.-M. *Acc. Chem. Res.* **2010**, *43*, 1019. (b) Huynh, M. H. V.; Meyer, T. J. *Chem. Rev.* **2007**, *107*, 5004. (c) Warren, J. J.; Tronic, T. A.; Mayer, J. M. *Chem. Rev.* **2010**, *110*, 6961. (d) Warren, J. J.; Mayer, J. M. *J. Am. Chem. Soc.* **2011**, *133*, 8544.
(6) (a) Fukuzumi, S. *Prog. Inorg. Chem.* **2009**, *56*, 49. (b) Fukuzumi, S. *Bull. Chem. Soc. Jpn.* **1997**, *70*, 1. (c) Fukuzumi, S.; Ohkubo, K. *Coord. Chem. Rev.* **2010**, *254*, 372.
(7) (a) Yoshikawa, S.; Shinzawa-Itoh, K.; Nakashima, R.; Yaono, R.; Yamashita, E.; Inoue, N.; Yao, M.; Fei, M. J.; Libeu, C. P.; Mizushima,

T.; Yamaguchi, H.; Tomizaki, T.; Tsukihara, T. *Science* **1998**, *280*, 1723. (b) Tsukihara, T.; Shimokata, K.; Katayama, Y.; Shimada, H.; Muramoto, K.; Aoyama, H.; Mochizuki, M.; Shinzawa-Itoh, K.; Yamashita, E.; Yao, M.; Ishimura, Y.; Yoshikawa, S. *Proc. Natl. Acad. Sci. U.S.A.* **2003**, *100*, 15304.

(8) Chufán, E. E.; Puiu, S. C.; Karlin, K. D. *Acc. Chem. Res.* **2007**, *40*, 563.

(9) (a) Collman, J. P.; Devaraj, N. K.; Decréau, R. A; Yang, Y.; Yan, Y.-L.; Ebina, W.; Eberspacher, T. A; Chidsey, C. E. D. *Science* **2007**, *315*, 1565. (b) Collman, J. P.; Decréau, R. A.; Lin, H.; Hosseini, A.; Yang, Y.; Dey, A.; Eberspacher, T. A. *Proc. Natl. Acad. Sci. U.S.A.* **2009**, *106*, 7320. (c) Collman, J. P.; Ghosh, S.; Dey, A.; Decréau, R. A.; Yang, Y. *J. Am. Chem. Soc.* **2009**, *131*, 5034.

(10) Rosenthal, J.; Nocera, D. G. *Acc. Chem. Res.* **2007**, *40*, 543.

(11) (a) Chang, C. J.; Loh, Z.-H.; Shi, C.; Anson, F. C.; Nocera, D. G. *J. Am. Chem. Soc.* **2004**, *126*, 10013. (b) Dogutan, D. K.; Stoian, S. A; McGuire, R.; Schwalbe, M.; Teets, T. S.; Nocera, D. G. *J. Am. Chem. Soc.* **2011**, *133*, 131. (c) Teets, T. S.; Cook, T. R.; McCarthy, B. D.; Nocera, D. G. *J. Am. Chem. Soc.* **2011**, *133*, 8114.

(12) (a) Askarizadeh, E.; Yaghoob, S. B.; Boghaei, D. M.; Slawin, A. M. Z.; Love, J. B. *Chem. Commun.* **2010**, *46*, 710. (b) Volpe, M.; Hartnett, H.; Leeland, J. W.; Wills, K.; Ogunshun, M.; Duncombe, B. J.; Wilson, C.; Blake, A. J.; McMaster, J.; Love, J. B. *Inorg. Chem.* **2009**, *48*, 5195.

(13) (a) Fukuzumi, S.; Okamoto, K.; Gros, C. P.; Guilard, R. *J. Am. Chem. Soc.* **2004**, *126*, 10441. (b) Fukuzumi, S.; Okamoto, K.; Tokuda, Y.; Gros, C. P.; Guilard, R. *J. Am. Chem. Soc.* **2004**, *126*, 17059.

(14) Kadish, K. M.; Frémond, L.; Shen, J.; Chen, P.; Ohkubo, K.; Fukuzumi, S.; El Ojaimi, M.; Gros, C. P.; Barbe, J.-M.; Guilard, R. *Inorg. Chem.* **2009**, *48*, 2571.

(15) (a) Hatay, I.; Su, B.; Li, F.; Méndez, M. A.; Khoury, T.; Gros, C. P.; Barbe, J.-M.; Ersoz, M.; Samec, Z.; Girault, H. H. *J. Am. Chem. Soc.* **2009**, *131*, 13453. (b) Partovi-Nia, R.; Su, B.; Li, F.; Gros, C. P.; Barbe, J.-M.; Samec, Z.; Girault, H. H. *Chem. Eur. J.* **2009**, *15*, 2335. (c) Hatay, I.; Su, B.; Méndez, M. A.; Corminboeuf, C.; Khoury, T.; Gros, C. P.; Bourdillon, M.; Meyer, M.; Barbe, J.-M.; Ersoz, M.; Zális, S.; Samec, Z.; Girault, H. H. *J. Am. Chem. Soc.* **2010**, *132*, 13733.

(16) (a) Partovi-Nia, R.; Su, B.; Méndez, M. A; Habermeyer, B.; Gros, C. P.; Barbe, J.-M.; Samec, Z.; Girault, H. H. *ChemPhysChem* **2010**, *11*, 2979. (b) Su, B.; Hatay, I.; Trojánek, A.; Samec, Z.; Khoury, T.; Gros, C. P.; Barbe, J.-M.; Daina, A.; Carrupt, P.-A.; Girault, H. H. *J. Am. Chem. Soc.* **2010**, *132*, 2655.

(17) (a) Fukuzumi, S.; Mochizuki, S.; Tanaka, T. *Inorg. Chem.* **1989**, *28*, 2459. (b) Fukuzumi, S.; Mochizuki, S.; Tanaka, T. *Inorg. Chem.* **1990**, *29*, 653. (c) Fukuzumi, S.; Mochizuki, S.; Tanaka, T. *J. Chem. Soc., Chem. Commun.* **1989**, 391.

(18) Fukuzumi, S. *Chem. Lett.* **2008**, *37*, 808.

(19) Kadish, K. M.; Shen, J.; Frémond, L.; Chen, P.; El Ojaimi, M.; Chkounda, M.; Gros, C. P.; Barbe, J.-M.; Ohkubo, K.; Fukuzumi, S.; Guilard, R. *Inorg. Chem.* **2008**, *47*, 6726.

(20) Ramdhanie, B.; Telser, J.; Caneschi, A.; Zakharov, L. N.; Rheingold, A. L.; Goldberg, D. P. *J. Am. Chem. Soc.* **2004**, *126*, 2515.

(21) Savéant, J.-M. *Chem. Rev.* **2008**, *108*, 2348.

(22) Halime, Z.; Kotani, H.; Li, Y.; Fukuzumi, S.; Karlin, K. D. *Proc. Natl. Acad. Sci. U.S.A.* **2011**, *108*, 13990.

(23) (a) Chen, R.; Li, H.; Chu, D.; Wang, G. *J. Phys. Chem. C* **2009**, *113*, 20689. (b) Shi, Z.; Zhang, J. *J. Phys. Chem. C* **2007**, *111*, 7084.

(24) Bakac, A. *Inorg. Chem.* **2010**, *49*, 3584.

(25) Zagal, J. H.; Griveau, S.; Silva, J. F.; Nyokong, T.; Bedioui, F. *Coord. Chem. Rev.* **2010**, *254*, 2755.

(26) (a) Li, Z. P.; Liu, B. H. *J. Appl. Electrochem.* **2010**, *40*, 475. (b) Zagal, J. H.; Gulppi, M.; Isaacs, M.; Cárdenas-Jirón, G.; Aguirre, M. J. *Electrochim. Acta* **1998**, *44*, 1349. (c) Li, W.; Yu, A.; Higgins, D. C.; Llanos, B. G.; Chen, Z. *J. Am. Chem. Soc.* **2010**, *132*, 17056.

(27) Gewirth, A. A.; Thorum, M. S. *Inorg. Chem.* **2010**, *49*, 3557.

(28) Honda, T.; Kojima, T.; Kobayashi, N.; Fukuzumi, S. *Angew. Chem., Int. Ed.* **2011**, *50*, 2725.

(29) (a) Yamada, Y.; Yoshida, S.; Honda, T.; Fukuzumi, S. *Energy Environ. Sci.* **2011**, *4*, 2822. (b) Jing, X.; Cao, D.; Liu, Y.; Wang, G.; Yin, J.; Wen, Q.; Gao, Y. *J. Electroanal. Chem.* **2011**, *658*, 46.

(30) Yamada, Y.; Fukunishi, Y.; Yamazaki, S.; Fukuzumi, S. *Chem. Commun.* **2010**, *46*, 7334.

(31) For metal−hydrogen peroxide semifuel cells, see: (a) Lei, T.; Tian, Y. M.; Wang, G. L.; Yin, J. L.; Gao, Y. Y.; Wen, Q.; Cao, D. X. *Fuel Cells* **2011**, *11*, 431. (b) Hasvold, O.; Storkersen, N.; Forseth, S.; Lian, T. *J. Power Sources* **2006**, *162*, 935. (c) Patrissi, C. J.; Bessette, R. R.; Kim, Y. K.; Schumacher, C. R. *J. Electrochem. Soc.* **2008**, *155*, B558.

(32) (a) Disselkamp, R. S. *Energy Fuels* **2008**, *22*, 2771. (b) Disselkamp, R. S. *Int. J. Hydrogen Energy* **2010**, *35*, 1049.

(33) (a) Galbács, Z. M.; Csányi, L. J. *J. Chem. Soc., Dalton Trans.* **1983**, 2353. (b) Latimer, W. M. In *The Oxidation States of the Elements and their Potentials in Aqueous Solutions*; Prentice-Hall: New York, 1952; p 39.

(34) (a) Abrantes, S.; Amaral, E.; Costa, A. P.; Shatalov, A. A.; Duarte, A. P. *Ind. Crop. Prod.* **2007**, *25*, 288. (b) Zeronian, S. H.; Inglesby, M. K. *Cellulose* **1995**, *2*, 265.

(35) Li, L.; Lee, S.; Lee, H. L.; Youn, H. J. *BioResoures* **2011**, *6*, 721.

(36) Armarego, W. L. F.; Chai, C. L. L. In *Purification of Laboratory Chemicals*, 5th ed.; Butterworth-Heinemann: Oxford, U.K., 2003.

(37) (a) Kobayashi, N.; Fukuda, T.; Ueno, K.; Ogino, H. *J. Am. Chem. Soc.* **2001**, *123*, 10740.

(38) DeSimone, R. E.; Drago, R. S. *J. Am. Chem. Soc.* **1970**, *92*, 2343.

(39) Altomare, A.; Burla, M.; Camalli, M.; Cascarano, G.; Giacovazzo, C.; Guagliardi, A.; Moliterni, A.; Polidori, G.; Spagna, R. *J. Appl. Crystallogr.* **1999**, *32*, 115.

(40) Burla, M. C.; Caliandro, R.; Camalli, M.; Carrozzini, B.; Cascarano, G. L.; De Caro, L.; Giacovazzo, C.; Polidori, G.; Spagna, R. *J. Appl. Crystallogr.* **2005**, *38*, 381.

(41) Flack, H. D. *Acta Crystallogr.* **1983**, *A39*, 876.

(42) (a) Ellis, P. E.; Linard, J. E.; Szymanski, T.; Jones, R. D.; Budge, J. R.; Basolo, F. *J. Am. Chem. Soc.* 1980, *102*, 1889. (b) Hill, A. V. *J. Physiol. (London)* **1910**, *40*, iv.

(43) Fukuzumi, S.; Kuroda, S.; Tanaka, T. *J. Am. Chem. Soc.* **1985**, *107*, 3020.

(44) Mann, C. K.; Barnes, K. K. In *Electrochemical Reactions in Non-aqueous Systems*; Marcel Dekker: New York, 1970.

(45) Fukuda, T.; Homma, S.; Kobayashi, N. *Chem. Eur. J.* **2005**, *11*, 5205.

(46) Kobayashi, N.; Nakajima, S.; Ogata, H.; Fukuda, T. *Chem. Eur. J.* **2004**, *10*, 6294.

(47) Canlıca, M.; Booysen, I. N.; Nyokong, T. *Polyhedron* **2011**, *30*, 522.

(48) Honda, T.; Kojima, T.; Fukuzumi, S. *Chem. Commun.* **2011**, *47*, 7986.

(49) Bernstein, P. A.; Lever, A. B. P. *Inorg. Chim. Acta* **1992**, *198*−*200*, 543.

(50) Kudrik, E. V.; Makarov, S. V.; Zahi, A.; van Eldik, R. *Inorg. Chem.* **2003**, *42*, 618.

(51) Loas, A.; Gerdes, R.; Zhang, Y.; Gorun, S. M. *Dalton Trans.* **2011**, *40*, 5162.

(52) Kumari, P.; Poonam; Chauhan, S. M. S. *Chem. Commun.* **2009**, 6397.

(53) Galezowski, W. *Inorg. Chem.* **2005**, *44*, 1530.

(54) Grodkowski, J.; Dhanasekaran, T.; Neta, P.; Hambright, P.; Brunschwig, B. S.; Shinozaki, K.; Fujita, E. *J. Phys. Chem. A* **2000**, *104*, 11332.

(55) Kobayashi, N.; Lam, H.; Nevin, W. A.; Janda, P.; Leznoff, C. C.; Lever, A. B. P. *Inorg. Chem.* **1990**, *29*, 3415.

(56) *CRC Handbook of Chemistry and Physics*, 89th ed.; Lide, D. R., Ed.; CRC Press: Boca Raton, FL, 2008−2009.

(57) Sawyer, D. T.; Valentine, J. S. *Acc. Chem. Res.* **1981**, *14*, 393.

(58) Under the conditions such that $k_{et1} \ll k_{et2}[HCOOH]$, a linear correlation between $k_{obs}(1 + K[HCOOH])/K$ and $[HCOOH]^2$ is predicted (see the detailed derivation on p S1 in the Supporting Information). The linear correlation between $k_{obs}(1 + K[HCOOH])/K$ and $[HCOOH]^2$ was obtained as shown in Figure S11 in Supporting Information. The k_{et2} value was determined from the slope of the linear plot of $k_{obs}(1 + K[HCOOH])/K$ vs $[HCOOH]^2$ to be $(4.9 \pm 0.2) \times 10^5$ M^{-2} s^{-1}.